RESEARCH ARTICLE
doi: 10.2306/scienceasia1513-1874.2025.100

ScienceAsia 51 (6): 2025: ID 2025100: **1–11**

Effects of hypoxia-induced mesenchymal stem cell-derived small extracellular vesicles on astrocytes subjected to oxygen-glucose deprivation/reperfusion injury

Ying Lyu[a,b,*], HongYan Wu[a], CunQuan Xiong[a], Xue Cao[a], PinPin Lu[c], Wei Chen[c], Pavithra Jayachandran[d], Sinouvassane Djearamane[e], Yongming Zhu[f], Yeong Hwang Tan[b], Ling Shing Wong[b]

[a] Jiangsu Medicine College, Yancheng, Jiangsu 224005 China
[b] Faculty of Health and Life Sciences, INTI International University, Nilai, Negeri Sembilan 71800 Malaysia
[c] Binhai County People's Hospital, Binhai, Jiangsu 224500 China
[d] Department of Chemistry, Sri Ramakrishna College of Engineering, Coimbatore, Tamilnadu 641022 India
[e] Department of Biomedical Science, Faculty of Science, Universiti Tunku Abdul Rahman, Kampar 31900 Malaysia
[f] College of Pharmaceutical Sciences, Soochow University, Suzhou, Jiangsu 215123 China

*Corresponding author, e-mail: lvying.1983@163.com

Received 11 Aug 2025, Accepted 7 Nov 2025
Available online 22 Dec 2025

ABSTRACT: Astrocyte injury is closely associated with the development of various neurological diseases. However, effective treatments remain limited. Given their nanoscale properties and capacity to penetrate the blood-brain barrier, small extracellular vesicles (sEVs) are potential candidates for therapy of astrocyte injury. The present study evaluated the neuroprotective potential of sEVs derived from rat bone marrow mesenchymal stem cells (rBMSCs) under hypoxicconditions. Using an *in vitro* model of oxygen-glucose deprivation/reperfusion (OGD/R) to mimic ischemia-reperfusion injury, the effects of hypoxia-induced rBMSCs-derived sEVs (MSC-sEVs) on injured astrocytes were investigated. After treatment, the cell viability, inflammatory mediator expression, and apoptotic signaling pathways of OGD/R-injured astrocytes were evaluated. The results showed that hypoxia-induced MSC-sEVs (H-sEVs) significantly enhanced astrocyte viability and mitigated inflammatory responses via upregulation of miR-21 expression, compared to the normal cultured rBMSCs-derived sEVs. The expression level of key pro-inflammatory mediators, including inducible nitric oxide synthase, interleukin-1 beta, tumor necrosis factor-alpha, and cyclooxygenase-2 were significantly attenuated. Apoptotic activity in astrocytes was reduced whereas anti-apoptotic B-cell lymphoma 2 protein expression in astrocytes was increased. These findings suggest that H-sEV may serve as a promising therapeutic strategy for ischemic stroke and other neuroinflammatory conditions.

KEYWORDS: hypoxia, mesenchymal stem cells, extracellular vesicles, astrocyte injury, ischemic stroke, ischemia-reperfusion, neuroprotection

INTRODUCTION

Small extracellular vesicles (sEVs) are nanoscale extracellular vesicles released from a variety of cells, such as immune cells, epithelial cells, and endothelial cells [1]. sEVs play a crucial role in intercellular communication, facilitating the transfer of signaling molecules and cargo between cells [2]. sEVs were identified many years ago and were initially reported as "platelet dust" in the blood [2]. Since then, extensive research has revealed their role in various physiological and pathological processes. sEVs have been linked to immune responses [3], tumor progression [4] and neurological disorders [5]. sEVs encapsulate abundant biomolecules such as DNA, messenger RNAs (mRNAs), microRNAs (miRNAs), proteins, and lipids [6]. Among these, miRNAs have gained significant attention due to their potent bioactivity and their crucial role in regulating gene expression. The therapeutic effects of sEVs are primarily mediated by the transfer of their molecular cargo, particularly the enriched miRNAs. These mature miRNAs are small, single-stranded non-coding RNAs, typically 20–25 nucleotides in length. They exert their regulatory influence by binding to the 3′-untranslated region (3′-UTR) of target mRNAs, leading to the repression of mRNA translation. This mechanism allows sEVs-derived miRNAs to precisely control a range of cellular processes, including proliferation, apoptosis, survival, and differentiation.

Cellular oxygen deprivation, or hypoxia, is a common physiologicaland pathological stress that necessitates a vigorous adaptation response. Under these circumstances, cells activate various complex responses designed to maintain life and homeostasis. A key component of this response is the regulated release of hypoxia-induced sEVs [7], a unique subset of sEVs whose molecular composition and functional properties markedly differ from those secreted under normoxic conditions [8]. These vesicles are particularly enriched with hypoxia-responsive factors, including vascular endothelial growth factor (VEGF), hypoxia-inducible factor-1α (HIF-1α), and a selective cohort of miRNAs, which together modulate vital pathways such as angiogenesis, metabolic adaptation, and immune regulation [9]. Increasing evidence suggests that the therapeutic potential of hypoxia-induced sEVs across a

range of preclinical disease models, including ischemic stroke [10], myocardial infarction [11], and neurodegenerative disorders [12].

Astrocytes, the predominant glial cells in the central nervous system, play indispensable roles in neuronal support and maintenance of neural homeostasis [13]. Dysfunction in astrocytes is increasingly implicated in the occurrence of numerous neurological disorders, including multiple sclerosis, Parkinson's disease, Alzheimer's disease, and ischemic stroke [13]. Ischemic stroke is defined as an impairment of blood supply to localized brain tissue, arising from a variety of etiological factors. Following injury induced by ischemic stroke, astrocytes undergo activation; through heterogeneous and progressive changes in their gene expression, morphology, proliferation, and function, these activated astrocytes—referred to as reactive astrocytes—exert protective effects [13, 14]. Despite advances in astrocyte biology, therapeutic strategies to mitigate astrocytic injury remain limited, primarily due to challenges in delivering treatments selectively to affected brain regions. Owing to their inherent ability to pass through the blood-brain barrier and target specific cell types, sEVs offer a promising vehicle for overcoming these delivery barriers [6]. As previously described, hypoxia-induced sEVs contain hypoxia-responsive factors which can inhibit apoptosis, induce neurogenesis and angiogenesis, and modulate inflammatory responses. While prior work [15] demonstrated that hypoxia-induced mesenchymal stem cell-derived sEVs (H-sEVs) promote functional recovery in spinal cord injury by shifting reactive astrocytes from an A1 to an A2 phenotype via the miR-21/JAK2/STAT3 pathway, their role in ischemia-reperfusion injury remains less understood. In particular, the effects of H-sEVs on astrocytes subjected to OGD/R, a condition relevant to stroke, especially with respect to detailed inflammatory and apoptotic signaling, have been unexplored.

This study investigates the protective effects of H-sEVs derived from rat bone marrow mesenchymal stem cells (rBMSCs) on oxygen-glucose deprivation/reperfusion (OGD/R)-injured astrocytes. It is hypothesized that these H-sEVs can attenuate astrocyte damage by modulating inflammatory pathways, enhancing cellular resilience, and promoting neurotrophic factor synthesis, compared to the normal cultured rBMSCs-derived sEVs (N-sEVs). To test this hypothesis, *in vitro* models of astrocytic injury were established by subjecting primary rat astrocytes to OGD/R, followed by treatment with H-sEVs. Then, the influences of H-sEVs treatment on astrocyte viability, inflammatory mediator expression, and anti-apoptotic effects were analyzed. The objectives of this study are to: (i) characterize the molecular cargo of H-sEVs including miRNAs; (ii) determine their effects on astrocyte viability and proliferation; (iii) elucidate their role in regulating astrocyte inflammatory responses; (iv) evaluate their capacity to modulate pro-inflammatory factor production; and (v) assess their efficacy in protecting astrocytes under OGD/R conditions.

MATERIALS AND METHODS

rBMSC characterization and hypoxia pretreatment

rBMSC and rat astrocyte primary culture were provided by Laboratory Animal Center of Soochow University. rBMSCs were cultured in DMEM/F12 medium (Gibco, New York, USA) supplemented with 10% FBS (Gibco) in a humidified incubator maintained at 37 °C and 5% CO_2, with medium changes every 2–3 days until they reached 80–90% confluence before subculturing. Phenotypic identity and purity of rBMSCs were confirmed by staining with fluorescently labeled antibodies (all from Invitrogen, Waltham, USA) targeting surface markers CD105 (1:200, 14-1051-82), CD90 (1:200, 17-0900-82), CD44 (1:200, 12-0441-82), and CD34 (1:200, 14-0341-82), followed by analysis using a flow cytometer (FACSCalibur; BD Biosciences, Seattle, USA).

To induce hypoxia, rBMSCs at the logarithmic growth stage were seeded in 60 mm dishes at a density of 5×10^5 cells per dish. Once 80% confluence was achieved, the medium was replaced with DMEM/F12 containing sEV-free serum and incubated in a hypoxic chamber with 2% O_2, 93% N_2, and 5% CO_2 at 37 °C for 48 h. After that, cultures from normoxic and hypoxic cultures were harvested and stored at 4 °C pending further analysis.

Cell viability assay of rBMSCs

To compare the metabolic activity of rBMSCs under hypoxic or normoxic conditions, cell viability was assessed using the cell counting kit 8 (CCK-8; Beyotime, Shanghai, China) over 6, 12, 24, and 48 h. Briefly, 10 µl of CCK-8 reagent was added to each well of microplate seeded with rBMSCs (2×10^3 cells/well), with five replicate wells per group and a blank control included. After 1-h incubation, absorbance at 450 nm was measured using a microplate reader (Perkin Elmer, Shelton, USA). The viability of BMSCs in each group was expressed as percentage relative to the 0-h time point.

sEVs isolation and identification

To remove the impurities, sEV-containing rBMSCs culture was centrifuged at 200×g for 5 min, followed by 20 min at 2,000×g, and 60 min at 10,000×g, all at 4 °C. sEVs were then isolated by ultracentrifugation at 100,000×g for 60 min at 4 °C and resuspended in sterile phosphate-buffered saline (PBS) for further analysis.

To confirm successful sEVs isolation, transmission electron microscopy (TEM; Hitachi, Tokyo, Japan) was used to visualize the morphology and size of the sEVs. Samples were negatively stainedusing 2% phosphotungstic acid to improve contrast for microscopy.

Then, TEM was used to observe the characteristic cup-shaped morphology of sEVs with a typical diameter ranging from 30 to 150 nm. The size distribution and isolated vesicle concentration were further analyzed by nanoparticle tracking analysis (NTA) with the nanoparticletracer device (Malvern Panalytical, Malvern, UK).

Western blotting was performed to confirm the presence of sEVs-specific protein. Briefly, protein concentration was quantified using a bicinchoninic acid (BCA) protein assay (Beyotime) and separated using sodium dodecyl sulfate polyacrylamide gel electrophoresis (SDS-PAGE). The membrane was blocked with 5% skim milk and incubated with primary antibodies (all from Abcam, Cambridge, USA) targeting CD9 (1:1000, ab263019), CD63 (1:1000, ab134045), Calnexin (1:1000, ab133615) and heat shock protein 90 (HSP90, 1:1000, ab53497), following by incubation with the HRP-conjugated secondary antibodies (HRP-Goat Anti-Mouse IgG and HRP-Goat Anti-Rabbit IgG) (1:1000, Beyotime). The protein bands were visualized using ECL detection kit and imaged with gel imager (Thermo Fisher Scientific, Waltham, USA).

RNA extraction and miR-21 quantification in sEVs

To investigate the effect of hypoxic treatment on the expression of miR-21 in isolated mesenchymal stem cell-derived small extracellular vesicles, total RNA was extracted from the sEVs using TRIzol reagent (Gibco). The extracted RNA was then reverse-transcribed into complementary DNA (cDNA) using a Bulge-Loop™ miRNA RT Kit (RiboBio, Guangzhou, China). The resulting cDNA served as a template for real-time quantitative PCR (RT-qPCR) on a RT- PCR instrument (Thermo Fisher Scientific).

The thermal cycling protocol was as follows: an initial pre-denaturation at 95 °C for 10 min, followed by 40 cycles of denaturation at 95 °C for 2 s, annealing at 60 °C for 20 s, and extension at 70 °C for 10 s. The mRNA expression levels were calculated using the comparative quantification method ($2^{-\Delta\Delta CT}$). U6 small nuclear RNA served as the internal control for the normalization of miR-21 expression levels.

Rat astrocyte primary culture and identification

Primary rat astrocyte cells were cultured in DMEM supplemented with 10% FBS and incubated in a humidified incubator at 37 °C with 5% CO_2. After 7–10 days cultivation, astrocytes were purified by shaking the flasks at 250 rpm for 18 h to detach astrocytes from microglia and oligodendrocyte precursor cells. Then, the supernatant was washed thrice with PBS for 5 min each, followed by fixation in 4% paraformaldehyde. After a 30-min fixation, the cells were rinsed again with PBS thrice for 5 min each. Non-specific binding sites were blocked by incubating the samples in 5% normal goat serum for 1 h. Thereafter, the samples were incubated with the primary antibody against glial fibrillary acidic protein (GFAP, 1:500, Biyuntian, China) followed by incubation in the dark for 2 h with Alexa Fluor 488-conjugated goat anti-mouse IgG secondary antibodies (Invitrogen, USA). Cell nuclei were counterstained with DAPI (Invitrogen, USA), and specimens were mounted with immunofluorescence mounting solution (Prolong Gold; Invitrogen). Fluorescent images were captured using a laser confocal fluorescence microscope (Nikon Corporation, Tokyo, Japan).

Rat astrocyte OGD/R and sEVs treatment

Astrocyte ischemia-reperfusion injury was modeled using an OGD/R protocol [16]. Astrocytes were exposed to 2 h of OGD by incubation in glucose- and serum-free DMEM under hypoxic conditions (1% O_2, 5% CO_2, 94% N_2), followed by a 4-h reoxygenation period with DMEM supplemented with 10% FBS under normoxic conditions (5% CO_2, 95% air). Then, astrocytes were treated with three different groups: (1) PBS as the negative control, (2) 5 μg/ml sEVs ($\sim 2\times10^9$ particles/ml) derived from normoxic rBMSCs, or (3) 5 μg/ml sEVs ($\sim 2\times10^9$ particles/ml) derived from hypoxia-induced rBMSCs. Untreated healthy astrocytes that were not subjected to the OGD/R protocol served as baseline control.

Cell viability of astrocytes

To investigate the impact of sEVs treatment on the OGD/R-injured astrocytes, cell viability of astrocytes was determined using the CCK-8 assay as described in Section “Cell viability assay of rBMSCs”.

Determination of inflammatory responses in astrocytes

To evaluate the inflammatory responses in astrocytes, we quantified the mRNA expression of key inflammatory mediators using RT-qPCR. Cultured astrocytes were lysed with TRIzol (Gibco), and RNA was extracted according to the manufacturer’s instructions. The quality of the extracted RNA was assessed by the OD260/OD280 ratio. For cDNA synthesis, the RiboBio Bulge-Loop™ miRNA RT Kit (RiboBio) was used. RT-qPCR was performed with the UltraSYBR mixture in a RT-PCR instrument (Thermo Fisher Scientific), using GAPDH as an internal control. The thermal cycling protocol was as follows: an initial pre-denaturation at 95 °C for 10 min, followed by 40 cycles of denaturation at 95 °C for 10 min, annealing at 60 °C for 10 s, and extension at 72 °C for 1 min. The mRNA expression levels were calculated using the comparative quantification method ($2^{-\Delta\Delta CT}$). The specific primers used for each target gene are listed in Table S1.

Terminal deoxynucleotidyl transferase dUTP nick end labeling (TUNEL) assay

Apoptosis of treated astrocytes was evaluated using the TUNEL apoptosis assay kit (Beyotime), in accordance with the manufacturer’s protocol. Briefly, cells were

initially fixed in 4% paraformaldehyde for 30 s at room temperature, followed by permeabilization with PBS solution containing 0.2% Triton X-100 at room temperature for 10 min. The TUNEL assay was then conducted to identify apoptotic cells. Fluorescence images were acquired using a Nikon laser confocal fluorescence microscope (Nikon Corporation). The 5 images were acquired from each well, 3 wells replicated in each experiment. The percentage of TUNEL-positive cells was calculated by the ratio of green positive cell number to the total cells (DAPI-labelled).

Western blotting for determination of Bcl-2 expression

The expression of a key anti-apoptotic protein, B-cell lymphoma 2 (Bcl-2) protein was determined using Western blotting. Protein extraction was carried out using radioimmunoprecipitation assay (RIPA) protein lysate (Beyotime) according to the manufacturer's protocol. Protein concentration was determined using a BCA protein assay kit and separated using SDS-PAGE. The membranes were blocked with 5% skim milk and incubated with primary antibodies from Cell Signaling, Beverly, USA against Bcl-2 (1:1000, 3498) and β-actin (1:1000, 58169), followed by incubation with HRP-conjugated secondary antibodies (HRP-Goat Anti-Mouse IgG and HRP-Goat Anti-Rabbit IgG, Beyotime) for 2 h at room temperature. Protein bands were visualized using an ECL detection kit and quantified using ImageJ software.

Data analysis

All the experiments were conducted in triplicate. The data analysis was performed using SPSS Statistics version 19.0 (IBM Corp., Armonk, NY, USA). Student's t-test and one-way analysis of variance (ANOVA) with Tukey's Honestly Significant Difference (HSD) test were employed to determine the significance. $p < 0.05$ was considered statistically significant. Results were presented as mean ± standard deviation (SD).

RESULTS AND DISCUSSION

Characterization of rBMSC and hypoxic pretreatment

To verify the phenotypic identity and purity of the rBMSCs, flow cytometry analysis was performed. Fig. 1a demonstrated that the rBMSCs showed high expression of CD105 and CD90 proteins, while exhibiting a lack of CD44 and CD34 expressions. These immunophenotypic characteristics align with the established criteria for BMSCs proposed by the International Society for Cellular Therapy [17]. Observation under inverted phase contrast microscopy also showed that rBMSCs were successfully cultured (Fig. S1) without contamination.

Fig. 1b illustrates the viability of rBMSCs after 6 h, 12 h, 24 h and 48 h of normoxic and hypoxic treatment. Across all time points, both normoxic and hypoxic treatments elicited a significant increase in rBMSC proliferation relative to 0 h. Notably, the rBMSCs cultured under hypoxic conditions exhibited enhanced proliferative capacity compared to the normoxic rBMSCs, with the most pronounced difference observed at 48 h. This observation was in agreement with Zhang et al [18], who reported a remarkable higher growth rate of rBMSCs under lower oxygen level compared to those at higher oxygen level.

sEVs isolation and identification

The extracted sEVs were characterized using TEM, NTA and Western blotting. Most sEVs isolated under both normoxic and hypoxic conditions exhibited the characteristic spherical morphology under TEM observation (Fig. 2a). NTA confirmed that sEVs from both conditions predominantly ranged in size from 50 to 150 nm (Fig. 2b). Notably, hypoxia-induced sEVs (H-sEVs) showed a larger mean diameter compared to their normoxia-induced sEVs (N-sEVs). This observation is consistent with prior reports. Zhu et al [11] identified a mean diameter of 136.5 nm for EVs from hypoxia-induced BMSCs, significantly larger than the 107.3 nm observed under normoxic conditions. Similar trends were also reported by Namazi et al [19]. Furthermore, Western blotting verified the presence of sEV markers, including CD9, CD63, and HSP90 (Fig. 2c), thereby confirming the identity of the isolated vesicles as sEVs [20]. In summary, these findings validate that the isolated particles possess the established morphological and molecular characteristics of sEVs.

miR-21 quantification in sEVs

To investigate the effects of hypoxic treatment on sEVs miR-21 expressions in rBMSCs, RT-qPCR was conducted. As illustrated in Fig. 3, H-sEVs exhibited a significant upregulation of miR-21 compared to those from normoxic control. This observation is consistent with previous research [21], suggesting that hypoxic stress may enhance the expression of miR-21 in sEVs as part of an adaptive response. Given the established roles of miR-21 in promoting cell survival, proliferation, and angiogenesis, the elevated miR-21 in sEVs content may underpin the enhanced therapeutic efficacy of sEVs to recipient cells [22]. Mechanistically, miR-21 is known to target and inhibit phosphatase and tensin homolog (PTEN), a critical negative regulator of the phosphatidylinositol 3-kinase (PI3K)/protein kinase B (Akt) signaling pathway and this key pathway is important for cellular survival, metabolism, and metastasis [23]. Thus, the enrichment of miR-21 in H-sEVs may facilitate astrocyte survival via activation of the PI3K/Akt signaling cascade.

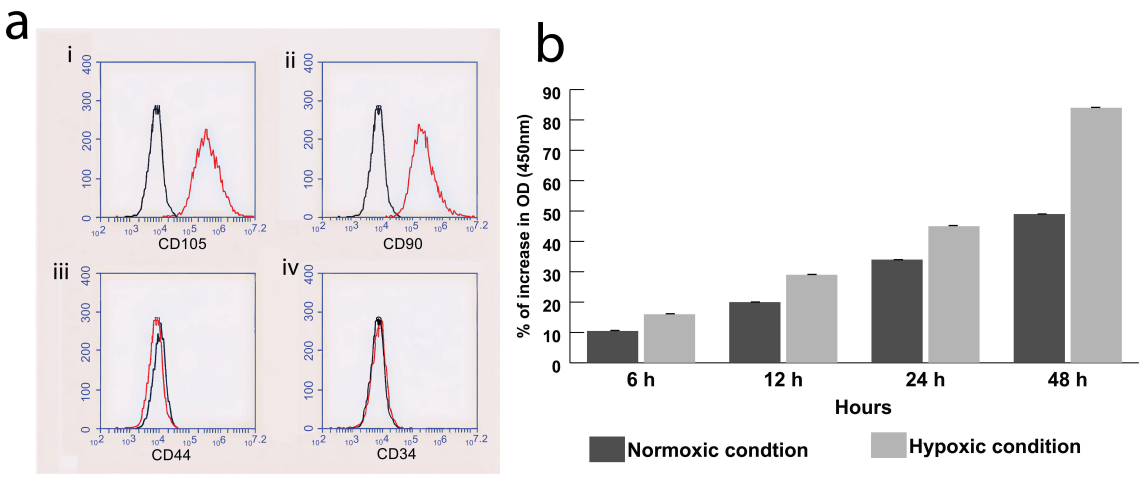

Fig. 1 Characterization of rBMSC. (a) The protein expression of surface markers in rBMSCs detected using flow cytometry ($n = 3$). (b) The cell viability of rBMSCs under normoxic and hypoxic conditions for 6, 12, 24 and 48 h. Viability was assessed using the CCK-8 assay and expressed as a percentage relative to the 0-h control. Data are presented as mean ± SD ($n = 5$).

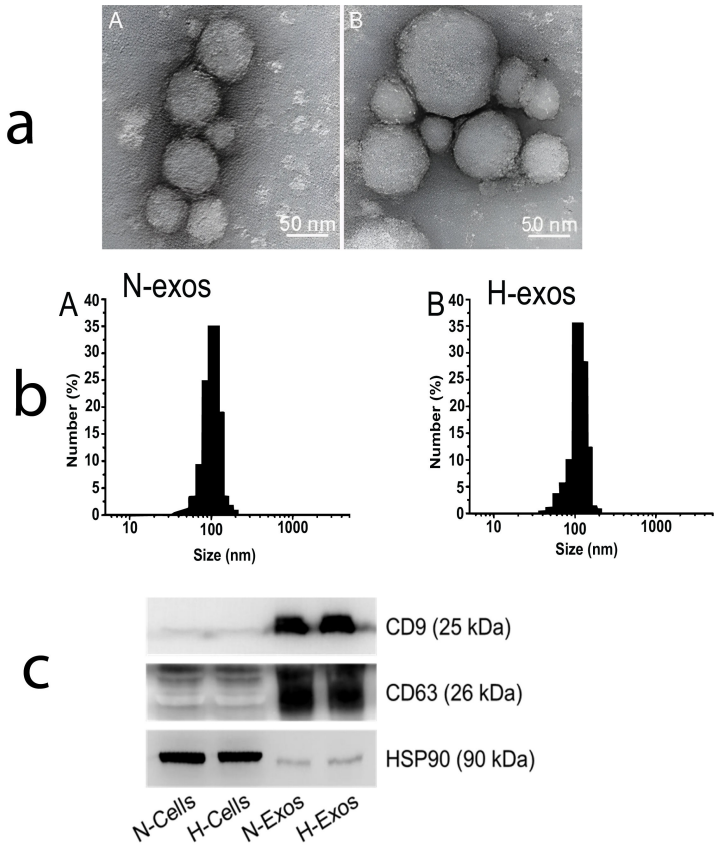

Fig. 2 Identification of exosome isolated under normoxic and hypoxic conditions. (a) TEM observation of sEVs: (A) N-sEVs, and (B) H-sEVs. (b) The particle size distribution of N-sEVs (N-Exos) and H-sEVs (H-Exos) using nanoparticle tracking analysis. (c) Western blotting image for the compilation of specific protein markers of CD9, CD63 and HSP90 in N-Exos and H-Exos. Negligible concentration of markers were expressed in the rBMSC samples under normal condition (N-Cells) and hypoxic condition (H-Cells).

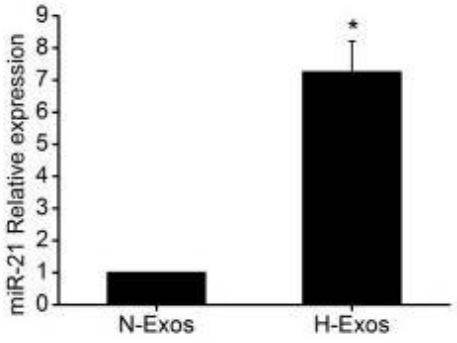

Fig. 3 Expression level of miR-21 in N-sEVs (N-Exos) and H-sEVs (H-Exos). Results are presented as mean ± SD ($n = 3$). Asterisk indicates a statistically significant difference between the groups ($p < 0.05$).

Rat astrocyte treatment with H-sEVs

Rat astrocyte primary culture and identification

To identify distinct cell populations within the samples, immunofluorescence staining was employed. Primary astrocytes were detected via indirect immunofluorescence using antibodies targeting GFAP and DAPI staining. As illustrated in Fig. 4a–c, the presence of DAPI nuclear staining confirmed that most of the GFAP-positive structures were indeed primary astrocytes. The purity of the isolated rat brain astrocyte cultures exceeded 95%.

sEVs treatment on rat astrocyte with OGD/R injure

To investigate the therapeutic potential of H-sEVs on astrocytes subjected to ischemia-reperfusion injury, an *in vitro* OGD/R model was established to simulate ischemia-reperfusion conditions [24]. Astrocytes exposed to OGD/R were subsequently treated with PBS without sEVs (control), N-sEVs, or H-sEVs. As shown in Fig. 5a, treatment with H-sEVs led to relative increase of miR-21 expression in astrocytes (2.49 ± 0.17), most likely due to EV-mediated transfer, whereas no significant change was observed in the PBS group (0.98 ± 0.04). Astrocytes treated with N-sEVs exhibited an intermediate miR-21 expression level (1.55 ± 0.26), which was higher than the PBS group but lower than the H-EVs group. This finding suggests that H-sEVs enhance miR-21 expression in astrocytes more effectively than those from normoxic conditions, potentially contributing to astrocyte protection and survival following ischemia-reperfusion injury.

To further assess the functional impact of these sEVs, cell viability was quantified using the CCK-8 assay after treatment. As shown in Fig. 5b, OGD/R injury significantly reduced astrocyte viability in the PBS-treated group without sEVs (OD450 of 0.38 ± 0.26). Treatment with N-Exos modestly improved cell viability (OD450 of 0.56 ± 0.03), while H-Exos conferred a more pronounced protective effect (OD450 of 0.73 ± 0.03). These results demonstrate that H-sEVs, which exhibited higher levels of miR-21, exerted a better neuroprotective effect compared to N-sEVs and untreated control. This is consistent with previous finding by Chen et al [25], who reported that H-sEVs enhanced miR-21 expression and cell viability in stressed βTC-6 pancreatic β-cells. The enhanced survival observed in astrocytes treated with H-sEVs may be attributed to several factors, including the aforementioned enrichment of miR-21 and the presence of other protective constituents within these sEVs, such as growth factors, anti-apoptotic proteins, and antioxidants, ultimately contributing to their cytoprotective properties [26]. However, another study by Jiang et al [27] reported conflicting results, showing that human umbilical vein endothelial cells (HUVEC)-derived EVs attenuate H/R-induced apoptosis by suppressing miR-21-3p and activating autophagy-related 12 (ATG12)-mediated autophagy. This discrepancy is likely attributable to several factors. Their study investigated miR-21-3p expression, while our study focused on miR-21-5p. Furthermore, different EV donors and recipient cell types were used across the two studies, leading to variations in target expression and downstream signaling. For instance, BMSC-derived EVs are known to carry neuroprotective miRNAs, such as miR-21-5p, miR-133b, and miR-210, as well as factors that promote cell survival and repair [28]. Supporting this, one study demonstrated that MSC-sEVs increased the rate of neurite growth, whereas EVs from umbilical cord sources did not [29]. Additionally, the different target cell types, neurons in their study versus astrocytes in ours, may have distinct basal miRNA expression profiles, different repertoires of target proteins, and varying sensitivities to apoptotic pathways. A single miRNA can exhibit a pro-apoptotic effect in one cell type but be neutral or protective in another due to differences in target protein abundance [30].

Next, the effect of inhibitory effect of MSC-EVs on pro-inflammatory in OGD/R-induced injured astrocytes was evaluated. The change of expression levels of the pro-inflammatory mRNA including tumor necrosis factor-alpha (TNF-α), interleukin-1 (IL-1β), cyclooxygenase-2 (COX-2), and nitric oxide synthase (iNOS) was determined using RT-PCR. Fig. 6 indicates that the expression levels of TNF-α, IL-1β, COX-2, and iNOS were upregulated in OGD/R-induced injured astrocytes without exosome treatment whereas the expression of these pro-inflammatory factors in the astrocytes was significantly suppressed by N-sEVs and H-sEVs. Moreover, compared with N-sEVs treatment, treatment with H-sEVs significantly decreased the expression of pro-inflammatory mRNAs level in OGD/R-injured astrocytes. This finding shows that H-sEVs strongly reduced the production of proinflammatory

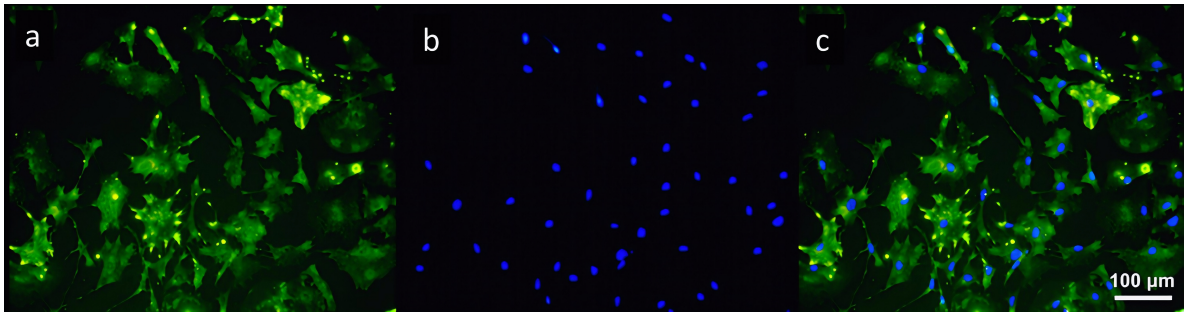

Fig. 4 Immunofluorescent labeling of rat astrocytes (a) GFAP labeled astrocytes, (b) DAPI labeled nuclei, and (c) overlay.

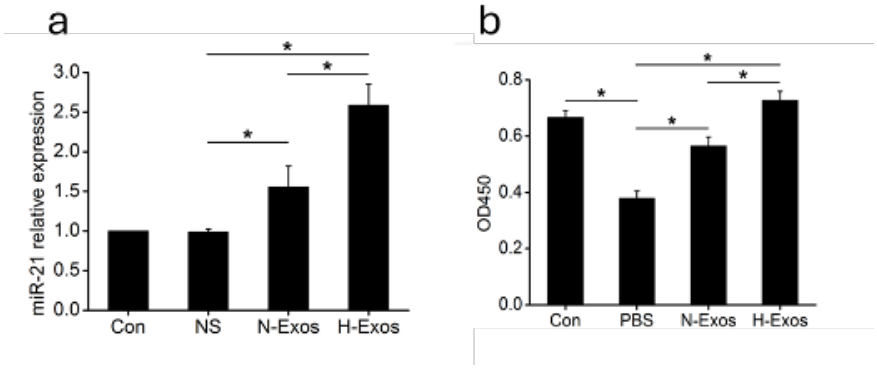

Fig. 5 Effect of different exosome treatments on OGD/R-injured astrocytes. (a) Expression level of miR-21 in OGD/R-injured astrocytes treated different groups of sEVs after 24 h of incubation ($n = 3$). (b) The cell viability of OGD/R-injured rat astrocytes treated with different groups of sEVs ($n = 3$). All the results are presented as mean ± SD. Asterisk indicates a statistically significant difference between the groups ($p < 0.05$).

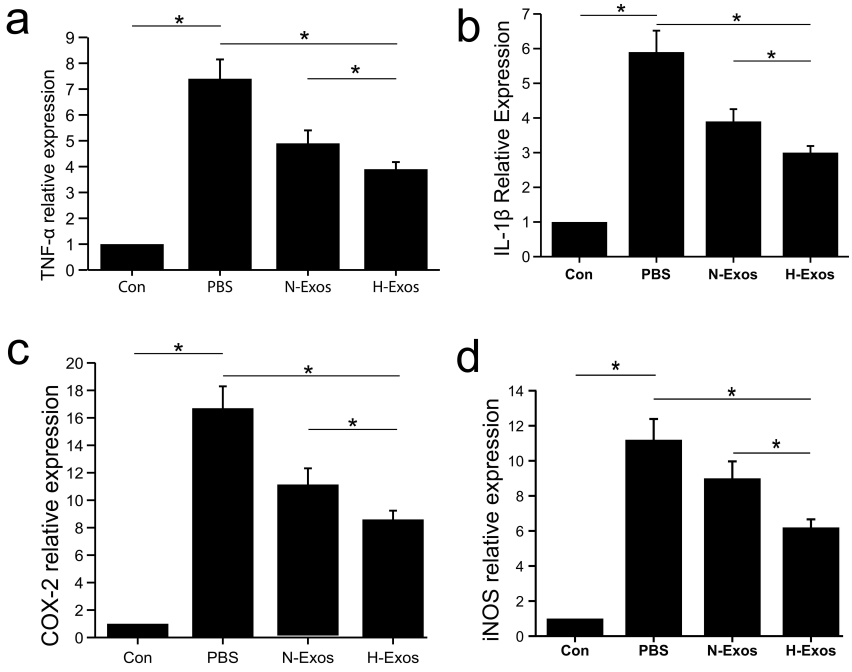

Fig. 6 Expression level of proinflammatory cytokines in OGD/R-injured astrocytes treated with different groups of sEVs. (a) TNF-α, (b) IL-1β, (c) COX-2, and (d) iNOS. Results are presented as mean ± standard deviations. Asterisk indicates a statistically significant difference between the groups ($p < 0.05$).

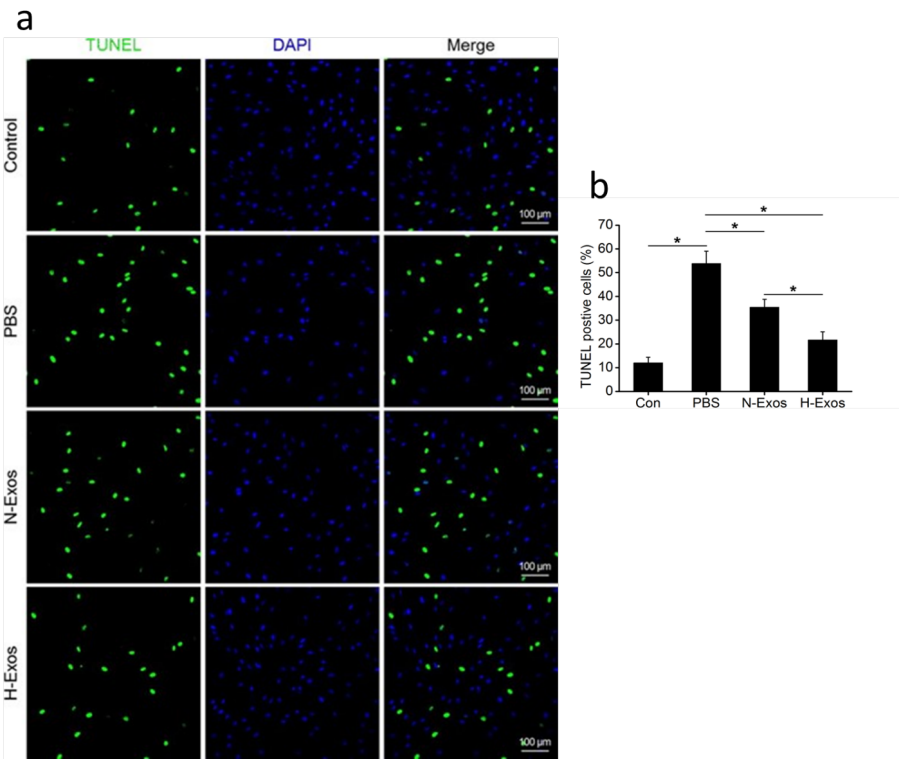

Fig. 7 Effect of different exosome treatments on apoptosis in OGD/R-injured astrocytes as assessed by (a) laser confocal fluorescence microscope and (b) TUNEL assay.

mediators in astrocytes injured by OGD/R, underscoring their anti-inflammatory properties. Inflammation plays a critical role in the occurrence of ischemic stroke-mediated neuronal damage and neurological abnormalities [31]. By suppressing the expression of these pro-inflammatory mediators, H-sEVs could inhibit the inflammatory response and mitigate the damage caused by OGD/R injury. This finding is consistent with the previous studies which demonstrated that sEVs could attenuate inflammation in various inflammatory conditions [32, 33]. The anti-inflammatory effects of sEVs may be attributed to its ability to modulate signaling pathways associated with inflammation [34]. Jiang et al [27] found that the downregulation of Programmed Cell Death 4 (PDCD4) by miR-21 promotes neurite outgrowth. Since PDCD4 is a known inhibitor of the NF-κB pathway, its suppression by miR-21 would lead to the activation of this pathway, resulting in a release of inflammatory mediators.

Apoptosis within the vulnerable ischemic penumbra is a significant consequence of cerebral ischemia/reperfusion injury [35]. Since the ischemic penumbra can still be reversible within the initial hours following the ischemic onset, timely reperfusion offers a critical opportunity to limit neuronal loss. Therefore, attenuating apoptosis in ischemic penumbra represents a critical therapeutic strategy. The findings of TUNEL assay (Fig. 7a) reveal a significant increase in apoptosis following OGD/R injury. Notably, astrocytes treated with N-sEVs showed a significant reduction in apoptosis, whereas astrocytes treated with H-sEVs exhibited an even more pronounced reduction in apoptosis (Fig. 7b). This finding aligns with the results reported by Chen et al [25], who reported the anti-apoptotic properties of EVs in pancreatic cell models.

To further elucidate the molecular mechanisms of MSC-EVs in attenuating apoptosis in rat astrocytes following OGD/R injury, expression of the anti-apoptotic Bcl-2 protein was investigated via Western blotting. As shown in Fig. 8, a significant upregulation of Bcl-2 expression was observed in astrocytes incubated with both N-sEVs and H-sEVs. Particularly, astrocytes treated with H-sEVs elicited a more pronounced increase in Bcl-2 expression compared to astrocytes treated with N-sEVs. This result suggests that sEVs derived under hypoxic conditions exhibited an enhanced capacity to promote Bcl-2 protein expression in astrocytes subjected to OGD/R damage, thereby conferring greater protection against apoptotic cell death.

Apoptosis is an important mechanism behind neuronal loss following ischemic stroke, ultimately leading to irreversible brain injury [36]. In this study, TUNEL assays confirmed that EVs derived from hypoxia-preconditioned rBMSCs significantly reduced OGD/R-

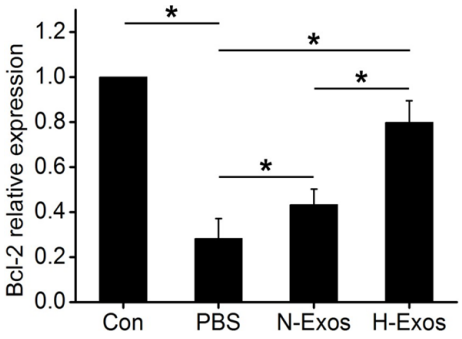

Fig. 8 Effect of different exosome treatments on apoptosis in OGD/R-injured astrocytes as assessed by Bcl-2 expression ($n = 3$). Results are presented as mean ± standard deviations. Asterisk indicates a statistically significant difference between the groups ($p < 0.05$).

induced apoptosis in astrocytes. This anti-apoptotic effect was correlated with a significant upregulation of the anti-apoptotic protein Bcl-2, suggesting that hypoxia-induced MSC-EVs help modulate the balance between pro- and anti-apoptotic signals. In parallel, these MSC-EVs substantially suppressed the expression of major pro-inflammatory mediators, including IL-1β, COX-2, and iNOS, resulting in reduction of neuroinflammation and its apoptotic consequences. A study revealed that sEVs from hypoxia-treated MSCs could regulate the miR-214-3p/PTEN, exerting a downregulating influence on the PTEN/Akt signaling pathway and promoting neuroprotection in ischemic stroke [37]. High levels of miR-21 expression in H-sEVs likely contribute to their protective effects by targeting PTEN. This action disinhibits the PI3K/Akt signaling pathway, which is a well-established mechanism for promoting cell survival and, in some contexts, enhancing specific inflammatory responses [38]. By repressing PTEN, miR-21 leads to increased phosphorylation and activation of Akt, a central node in cell survival signaling. This activation promotes cell growth and metabolism while inhibiting apoptosis through the upregulation of anti-apoptotic factors and the downregulation of pro-apoptotic factors. This pathway is a critical component for both cell survival and tissue regeneration following injury [39]. Simultaneously, miR-21 directly targets and downregulates PDCD4 mRNA. Because PDCD4 is an inhibitor of the NF-κB pathway, its suppression by miR-21 consequently activates the NF-κB pathway. As a central regulator of inflammatory responses, the NF-κB pathway's activation is directly linked to a reduction in key pro-inflammatory mediators such as iNOS, IL-1β, TNF-α, and COX-2 [40]. miR-2 has also been shown to be a strong anti-apoptosis and pro-survival factor in ischemia. miR-21 could regulate ischemic neuronal injury via the p53/Bcl-2/Bax signaling pathway [40].

Together, these distinct mechanisms driven by miR-21 ultimately produce anti-inflammatory and pro-survival effects in OGD/R astrocytes.

CONCLUSION

This study provides compelling evidence for the neuroprotective potential of H-sEVs in mitigating OGD/R injury in astrocytes. These H-sEVs significantly enhanced astrocyte viability via multiple mechanisms. Functional investigations revealed the miR-21 expression was upregulated in OGD/R-injured astrocytes following H-sEVs treatment, suggesting a key contribution to astrocyte protection and survival against inflammatory responses. In parallel, these H-sEVs effectively suppressed the production of pro-inflammatory mediators such as TNF-α, IL-1β, COX-2, and iNOS, highlighting their potent immunomodulatory effects. Additionally, H-sEVs treatment led to a substantial reduction in apoptotic cell death, coinciding with elevated Bcl-2 expression and preserved cellular integrity in OGD/R-injured astrocytes. In conclusion, these results suggest that H-sEVs represent a promising therapeutic strategy for ischemic strokes and other neurological disorders characterized by ischemia-reperfusion injury. Future research should focus on the identification and functional characterization of specific bioactive cargo within these sEVs. Rigorous pre-clinical studies are also essential to facilitate the translation of these compelling findings into clinical applications.

Appendix A. Supplementary data

Supplementary data associated with this article can be found at https://dx.doi.org/10.2306/scienceasia1513-1874.2025.100.

Acknowledgements: This research was supported by Jiangsu Province Vocational Education Teachers' Teaching Innovation Team Construction Project (2021), Outstanding Young Backbone Teachers of Jiangsu Universities under the 'Blue and Blue Project' (2021), Jiangsu Higher Education Institution Innovative Research Team for Science and Technology (2023), and Jiangsu Province Engineering Research Center for Cardiovascular and Cerebrovascular Disease and Cancer Prevention and Control (2022). The authors also would like to gratefully acknowledge the materials, facilities and technical support provided by Soochow University. The data used in this study were obtained using research instruments and resources at Soochow University, and we thank the institution for granting access to these facilities.

REFERENCES

1. Théry C, Ostrowski M, Segura E (2009) Membrane vesicles as conveyors of immune responses. *Nat Rev Immunol* **9**, 581–593.
2. Hessvik NP, Llorente A (2018) Current knowledge on exosome biogenesis and release. *Cell Mol Life Sci* **75**, 193–208.
3. Essola JM, Zhang M, Yang H, Li F, Xia B, Mavoungou JF, Hussain A, Huang Y (2024) Exosome regulation of immune response mechanism: Pros and cons in immunotherapy. *Bioact Mater* **32**, 124–146.

4. Tai YL, Chen KC, Hsieh JT, Shen TL (2018) Exosomes in cancer development and clinical applications. *Cancer Sci* **109**, 2364–2374.
5. Alvarez-Erviti L, Seow Y, Yin H, Betts C, Lakhal S, Wood MJA (2011) Delivery of siRNA to the mouse brain by systemic injection of targeted exosomes. *Nat Biotechnol* **29**, 341–345.
6. Metheetrirut C, Khowawisetsut L, Nonsuwan P, Punnakitikashem P, Pattanapanyasat K (2025) Extracellular vesicles: A comprehensive review of classification, isolation, characterization, and cargo loading. *ScienceAsia* **51S**, ID 2025s007.
7. Manuel GE, Johnson T, Liu D (2017) Therapeutic angiogenesis of exosomes for ischemic stroke. *Int J Physiol Pathophysiol Pharmacol* **9**, 188–191.
8. Belting M, Christianson HC (2015) Role of exosomes and microvesicles in hypoxia-associated tumour development and cardiovascular disease. *J Intern Med* **278**, 251–263.
9. Jiang H, Zhao H, Zhang M, He Y, Li X, Xu Y, Liu X (2022) Hypoxia induced changes of exosome cargo and subsequent biological effects. *Front Immunol* **13**, 824188.
10. Li Y, Ren C, Li H, Jiang F, Wang L, Xia C, Ji X (2019) Role of exosomes induced by remote ischemic preconditioning in neuroprotection against cerebral ischemia. *Neuroreport* **30**, 834–841.
11. Zhu LP, Tian T, Wang JY, He JN, Chen T, Pan M, Xu L, Zhang H, et al (2018) Hypoxia-elicited mesenchymal stem cell-derived exosomes facilitates cardiac repair through miR-125b-mediated prevention of cell death in myocardial infarction. *Theranostics* **8**, 6163–6177.
12. Gao P, Li X, Du X, Liu S, Xu Y (2021) Diagnostic and therapeutic potential of exosomes in neurodegenerative diseases. *Front Aging Neurosci* **13**, 790863.
13. Shen XY, Gao ZK, Han Y, Yuan M, Guo YS, Bi X (2021) Activation and role of astrocytes in ischemic stroke. *Front Cell Neurosci* **15**, 755955.
14. Xu H, Chen M (2022) Berberine ameliorates lipopolysaccharide-induced astrocyte activation and migration via NDUFC2. *ScienceAsia* **48**, 406–413.
15. Yang Z, Liang Z, Rao J, Xie H, Zhou M, Xu X, Lin Y, Lin F, et al (2024) Hypoxic-preconditioned mesenchymal stem cell-derived small extracellular vesicles promote the recovery of spinal cord injury by affecting the phenotype of astrocytes through the miR-21/JAK2/STAT3 pathway. *CNS Neurosci Ther* **30**, e14428.
16. Ma Y, Zhao P, Zhu J, Yan C, Li L, Zhang H, Zhang M, Gao X, et al (2016) Naoxintong protects primary neurons from oxygen-glucose deprivation/reoxygenation induced injury through PI3K-Akt signaling pathway. *Evid Based Complement Alternat Med* **2016**, 5815946.
17. Dominici M, Le Blanc K, Mueller I, Slaper-Cortenbach I, Marini FC, Krause DS, Deans RJ, Keating A, et al (2006) Minimal criteria for defining multipotent mesenchymal stromal cells. The International Society for Cellular Therapy position statement. *Cytotherapy* **8**, 315–317.
18. Zhang J, Xiong L, Tang W, Tang L, Wang B (2018) Hypoxic culture enhances the expansion of rat bone marrow-derived mesenchymal stem cells via the regulatory pathways of cell division and apoptosis. *Vitr Cell Dev Biol Anim* **54**, 666–676.
19. Namazi H, Namazi I, Ghiasi P, Ansari H, Rajabi S, Hajizadeh-Saffar E, Aghdami N, Mohit E (2018) Exosomes secreted by normoxic and hypoxic cardiosphere-derived cells have anti-apoptotic effect. *Iran J Pharm Res* **17**, 377–385.
20. Ono K, Sogawa C, Kawai H, Tran MT, Taha EA, Lu Y, Oo MW, Okusha Y, et al (2020) Triple knockdown of CDC37, HSP90-alpha and HSP90-beta diminishes extracellular vesicles-driven malignancy events and macrophage M2 polarization in oral cancer. *J Extracell Vesicles* **9**, 1769373.
21. Charlotte Zoe A, Stafford MYC, McNally CJ, Heather N, Declan JM (2023) MiR-21 Is induced by hypoxia and down-regulates RHOB in prostate cancer. *Cancers (Basel)* **15**, 1291.
22. Mayourian J, Ceholski DK, Gorski PA, Mathiyalagan P, Murphy JF, Salazar SI, Stillitano F, Hare JM, et al (2018) Exosomal microRNA-21-5p mediates mesenchymal stem cell paracrine effects on human cardiac tissue contractility. *Circ Res* **122**, 933–944.
23. Li Y, Tan J, Miao Y, Zhang Q (2021) MicroRNA in extracellular vesicles regulates inflammation through macrophages under hypoxia. *Cell Death Discov* **7**, 285.
24. Li J, Yang C, Wang Y (2021) miR-126 overexpression attenuates oxygen-glucose deprivation/reperfusion injury by inhibiting oxidative stress and inflammatory response via the activation of SIRT1/Nrf2 signaling pathway in human umbilical vein endothelial cells. *Mol Med Rep* **23**, 165.
25. Chen J, Chen J, Cheng Y, Fu Y, Zhao H, Tang M, Zhao H, Lin N, et al (2020) Mesenchymal stem cell-derived exosomes protect beta cells against hypoxia-induced apoptosis via miR-21 by alleviating ER stress and inhibiting p38 MAPK phosphorylation. *Stem Cell Res Ther* **11**, 97.
26. Jiao YR, Chen KX, Tang X, Tang YL, Yang HL, Yin YL, Li CJ (2024) Exosomes derived from mesenchymal stem cells in diabetes and diabetic complications. *Cell Death Dis* **15**, 271.
27. Jiang Y, Xie H, Tu W, Fang H, Ji C, Yan T, Huang H, Yu C, et al (2018) Exosomes secreted by HUVECs attenuate hypoxia/reoxygenation-induced apoptosis in neural cells by suppressing miR-21-3p. *Am J Transl Res* **10**, 3529–3541.
28. Nasirishargh A, Kumar P, Ramasubramanian L, Clark K, Hao D, Lazar SV, Wang A (2021) Exosomal microRNAs from mesenchymal stem/stromal cells: Biology and applications in neuroprotection. *World J Stem Cells* **13**, 776–794.
29. Lopez-Verrilli MA, Caviedes A, Cabrera A, Sandoval S, Wyneken U, Khoury M (2016) Mesenchymal stem cell-derived exosomes from different sources selectively promote neuritic outgrowth. *Neuroscience* **21**, 129–139.
30. Wang B, Yu P, Lin W, Zhai Z (2021) MicroRNA-21-5p reduces hypoxia/reoxygenation-induced neuronal cell damage through negative regulation of CPEB3. *Anal Cell Pathol (Amst)* **2021**, 5543212.
31. Iadecola C, Anrather J (2011) The immunology of stroke: from mechanisms to translation. *Nat Med* **17**, 796–808.
32. Xia C, Zeng Z, Fang B, Tao M, Gu C, Zheng L, Wang Y, Shi Y, et al (2019) Mesenchymal stem cell-derived exosomes ameliorate intervertebral disc degeneration via anti-oxidant and anti-inflammatory effects. *Free Radic Biol Med* **143**, 1–15.

33. Oyar EO, Aciksari A, Azak Pazarlar B, Egilmez CB, Duruksu G, Rencber SF, Yilmaz MY, Ozturk A, et al (2022) The therapeutical effects of damage-specific stress induced exosomes on the cisplatin nephrotoxicity *in vivo*. *Mol Cell Probes* **66**, 101861.
34. Zhang PY, Wu P, Khan UZ, Zhou Z, Sui X, Li C, Dong K, Liu Y, et al (2023) Exosomes derived from LPS-preconditioned bone marrow-derived MSC modulate macrophage plasticity to promote allograft survival via the NF-κB/NLRP3 signaling pathway. *J Nanobiotechnology* **21**, 332.
35. Zhang Q, Jia M, Wang Y, Wang Q, Wu J (2022) Cell death mechanisms in cerebral ischemia-reperfusion injury. *Neurochem Res* **47**, 3525–3542.
36. Broughton BRS, Reutens DC, Sobey CG (2009) Apoptotic mechanisms after cerebral ischemia. *Stroke* **40**, e331–e339.
37. Wu Q, Wu JH, Ye ZY, She W, Peng WJ, Zhang HX, Qi C, Tian T, et al (2024) Exosomes from hypoxia-treated mesenchymal stem cells: Promoting neuroprotection in ischemic stroke through miR-214-3p/PTEN mechanism. *Mol Neurobiol* **61**, 7611–7626.
38. Gao X, Xiong Y, Li Q, Han M, Shan D, Yang G, Zhang S, Xin D, et al (2020) Extracellular vesicle-mediated transfer of miR-21-5p from mesenchymal stromal cells to neurons alleviates early brain injury to improve cognitive function via the PTEN/Akt pathway after subarachnoid hemorrhage. *Cell Death Dis* **11**, 363.
39. Shi B, Wang Y, Zhao R, Long X, Deng W, Wang Z (2018) Bone marrow mesenchymal stem cell-derived exosomal miR-21 protects C-kit$^+$ cardiac stem cells from oxidative injury through the PTEN/PI3K/Akt axis. *PLoS One* **13**, e0191616.
40. Yan H, Huang W, Rao J, Yuan J (2021) miR-21 regulates ischemic neuronal injury via the p53/Bcl-2/Bax signaling pathway. *Aging (Albany NY)* **13**, 22242–22255.

Appendix A. Supplementary data

Table S1 Primer sequences for RT-qPCR of key inflammatory mediators.

Gene	Primer sequences	
TNF-α	Forward primer (5′–3′)	CTCTTCTCATTCCTGCTCGT
	Reverse primer (5′–3′)	CATTTGGGAACTTCTCCTCC
IL-1β	Forward primer (5′–3′)	ATGGCAACTGTTCCTGAACTC
	Reverse primer (5′–3′)	TTAGGAAGACACGGATTCCAT
COX-2	Forward primer (5′–3′)	TGTATGCTACCATCTGGCTTCGG
	Reverse primer (5′–3′)	GTTTGGAACAGTCGCTCGTCATC
iNOS	Forward primer (5′–3′)	CACCACCCTCCTTGTTCAAC
	Reverse primer (5′–3′)	CAATCCACAACTCGCTCCAA
GAPDH	Forward primer (5′–3′)	GGCACAGTCAAGGCTGAGAATG
	Reverse primer (5′–3′)	ATGGTGGTGAAGACGCCAGTA

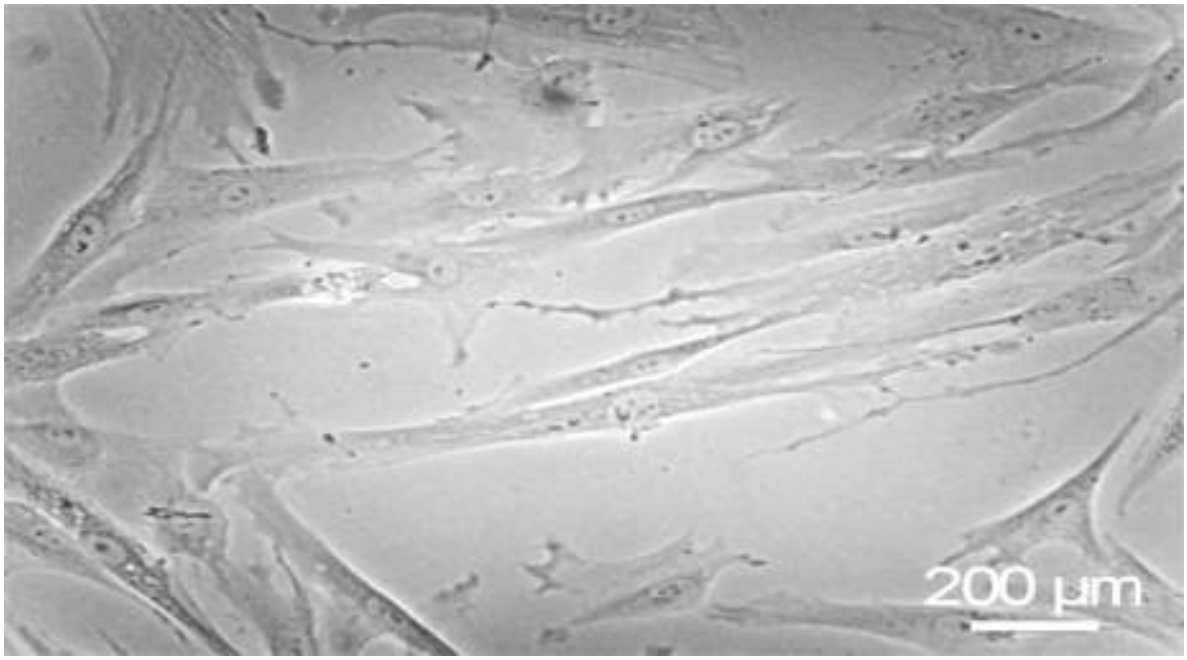

Fig. S1 Microscopic observation of rBMSC culture with magnification ×1000 using inverted phase contrast microscopy. The rBMSCs were identified by fibroblast- like morphology with polygonal spindle shapes, which were tightly arranged in monolayer.